Electron paramagnetic resonance investigations of α-Al_2O_3 powders doped with Fe^{3+} ions: experiments and simulations

2002 J. Phys.: Condens. Matter 14 10331

(http://iopscience.iop.org/0953-8984/14/43/329)

INSTITUTE OF PHYSICS PUBLISHING JOURNAL OF PHYSICS: CONDENSED MATTER

J. Phys.: Condens. Matter **14** (2002) 10331–10348 PII: S0953-8984(02)38039-1

Electron paramagnetic resonance investigations of α-Al_2O_3 powders doped with Fe^{3+} ions: experiments and simulations

J Y Buzaré[1], G Silly[1], J Klein[2], G Scholz[2], R Stösser[2] and M Nofz[3]

[1] Laboratoire de Physique de l'Etat Condensé UMR CNRS no 6087, Université du Maine, Av. Olivier Messiaen, F-72085 Le Mans, Cedex 9, France
[2] Humboldt-Universität zu Berlin, Institut für Chemie, Brook-Taylor-Strasse 2, D-12489, Berlin, Germany
[3] Bundesanstalt für Materialforschung und -prüfung, 12000 Berlin, Germany

Received 12 June 2002
Published 18 October 2002
Online at stacks.iop.org/JPhysCM/14/10331

Abstract

Electron paramagnetic resonance (EPR) of Fe^{3+} ions in Al_2O_3 is studied in powder samples prepared by different routes and/or modified by thermal or mechanical treatments, with different doping levels and grain sizes. The measurements are performed in various frequency bands (S, X, K, Q and W) and with bimodal detection in X-band. Simulations of the spectra are achieved with a code designed for computing EPR powder spectra described by any spin Hamiltonian including second-, fourth- and sixth-order ZFS terms ($S \leqslant 7/2$). The linewidths, intensities and lineshapes are accounted for. The lineshape is Gaussian at low Fe^{3+} concentration whereas it is Lorentzian for higher concentration. The linewidths are interpreted as the superimposition of three main contributions: intrinsic linewidth, dipolar broadening and broadening due to lattice imperfections. The latter is tentatively interpreted in terms of quadrupolar spin Hamiltonian parameter distributions treated using first-order perturbation theory. Whatever the sample, only the b_2^2 spin Hamiltonian parameter is found to be distributed around a mean zero value which corresponds to rhombic distortions. Angle and bond length distributions are tentatively extracted from the b_2^2 distributions which gives some insight into the local order around the spin probe in relation to the preparation and treatment of the samples.

1. Introduction

It is well known that mechanical, electric and magnetic properties of oxide ceramic materials such as alumina may be changed significantly by doping with small concentrations of transition metal ions (i.e. Cr^{3+}, Fe^{3+}) [1]. Moreover, these ions may be used as sensitive electron

paramagnetic resonance (EPR) probes of their local environment [2–4]. In this way EPR allows us to study the site distribution of the probes.

As alumina ceramics with various grain sizes and resulting from different syntheses (dehydration, mechanical milling, film deposition, thermal treatments, soft chemical routes) are widely used in modern technological processes, it is important to investigate transition metal ions in these materials in order to analyse quantitatively the interaction of the ion with the lattice, the localization of the ion and the real local structure around this ion. Furthermore, as in the field of nanostructured materials, nano alumina powder is one of the most important fine materials and particular attention may be paid to local structure modifications induced by the preparation route (e.g. mechanical milling [5]). Therefore, EPR spectroscopy can be used in parallel and as a complementary method with classical methods of structural analysis such as x-ray, neutron diffraction or TEM. It is recognized as a powerful tool for solid state investigation due to its low detection threshold and its structural sensitivity to local ligand fields.

In order to reach this goal, it is necessary to quantify the sensitivity of the paramagnetic probes to the possible structural changes of their neighbourhood in relation with those of the matrix itself. It was previously shown [6–8] that EPR linewidth measurements can be used to determine small concentrations of Fe^{3+} and Cr^{3+} dopants and grain sizes in commercially available Al_2O_3 samples. In these works, no attempts were made to relate the results to distributions of spin Hamiltonian parameters. More recent works [5, 9–12] suggest that the EPR linewidth broadening may be interpreted partly in term of narrow spin Hamiltonian parameter distributions reflecting small fluctuations in the local symmetry. Statistical distributions (program ESR-MAKRO_1 [11]) were used to describe the effect of milling in Fe^{3+} doped α-Al_2O_3 and tentatively related to local disorder [5]. Furthermore, Priem *et al* [12] demonstrate that multifrequency EPR is well suited for the determination of zero field splitting (ZFS) parameters.

It is the aim of this paper to report on EPR measurements on Al_2O_3 powders prepared by various routes, on the determination of the spin Hamiltonian parameters and their distributions in order to gain a deeper insight into the local structure of the different samples and to demonstrate that EPR is a valuable tool to investigate modified alumina.

We focus on the Fe^{3+} ion, which is one of the most sensitive spin probes. This ion substitutes for Al^{3+} and is very well detectable. Due to the similarity of the Fe^{3+} and Al^{3+} ionic radii ($R_{Fe^{3+}} = 0.65$ Å, $R_{Al^{3+}} = 0.53$ Å) [13] and the equality in their charges, Fe^{3+} is usually expected to disturb the matrix to a negligible extent from a geometrical point of view with no local charge compensation. Its spectrum is well known [2, 3] at least in X-band and, furthermore, the fine structure of the ^6S (Fe^{3+}) ground state should reflect sensitively local changes such as arrangements and distances in the corresponding coordination polyhedra. Due to the trigonal space group of the undisturbed crystalline corundum matrix there is *per definitionem* no rhombic component of the local electric potential. Therefore, any distortion leading to a deviation from the original symmetry should be reflected sensitively by the appearance of nonzero rhombic components of the local electric fields.

After describing the experimental and theoretical methods carried out in this work, we will present:

(i) calculations of powder spectra of α-Al_2O_3:Fe^{3+} showing the influence of selected ZFS parameters and their statistical distributions on the positions and intensities of the resonance transitions;

(ii) a discussion on what kind of complementary information can be obtained about the spin system choosing different frequency bands with the usual detection mode with the microwave perpendicular to the static magnetic field B_0 ($B_1 \perp B_0$) as well as detection in the mode with $B_1 \parallel B_0$.

(iii) measurements of EPR spectra of α-Al_2O_3:Fe^{3+} in several microwave frequency bands, determination of spin Hamiltonian parameters and their distributions in real samples corresponding to different preparation routes, and
(iv) finally, a quantitative description of the degree of local distortions of the matrix by applying the superposition model [14–18] for the interpretation of the EPR ZFS parameters of Fe^{3+} ions in different corundum samples.

2. Experimental and theoretical methods

2.1. Materials

The corundum powders used for the present investigations exhibit different levels of Fe^{3+} concentration and various mean particle sizes. They also correspond to different preparation routes. The samples are presented below.

Sample I. α-Al_2O_3 (99.99%) obtained from Aldrich Chem. Co., Inc. Fe^{3+} ions allowing ESR spectroscopic measurements are present in the matrix as impurities (2×10^{-4} mol% Fe_2O_3 per mole Al_2O_3, certificate of analysis, mean particle size: 350 nm);

Sample II. α-Al_2O_3 (CT 3000 SG, Alcoa Co., 0.02 mol% Fe_2O_3);

Samples III–V. were prepared by a sol–gel route (Yoldas procedure [19, 20]) starting from Al-sec-butylate. The Fe^{3+} doped boehmite sols were gelled, dried and heated in DTA equipment up to 1200 °C (heating rate: 10 K min^{-1}) and finally quenched. They have a content of 0.26, 0.52 and 1.04 mol% Fe_2O_3, respectively.

In addition, further samples were prepared by thermal annealing and mechanical milling starting from sample I and by thermal annealing from sample II.

The thermal annealing was performed in quasi-closed Pt crucibles for a time–temperature regime of (i) 14 h at 1300 °C and subsequently (ii) 7.5 h at 1500 °C.

2.2. Measurements

The measurements were performed with an EPR X-band spectrometer ERS 300 (ZWG Berlin-Adlershof, Germany) at room temperature. Q-band and S-band measurements were performed with the microwave bridges ER051QG (cavity ER5106QT) and ER061SY, respectively (Bruker, Germany) which were adapted to the ERS 300 spectrometer. W-band measurements were performed with the commercial Bruker cw spectrometer E600.

2.3. Computation of EPR spectra

The ZFS parameters of the Fe^{3+} ions ($S = 5/2$) were determined using the simulation program EPR-ULM [21] which is based on the complete diagonalization of the spin Hamiltonian matrix. The EPR-ULM code is designed for computing EPR powder spectra described by any spin Hamiltonian including second-, fourth- and sixth-order ZFS terms ($S \leqslant 7/2$). The general form of the ZFS Hamiltonian for arbitrary low symmetry in terms of extended Stevens operators [22] is given by

$$\hat{\boldsymbol{H}}_{ZFS} = \sum_{k,q} f_k b_k^q O_k^q$$

with $k = 2, 4$ and 6, $-k \leqslant q \leqslant k$, $f_k = 1/3, 1/60$ and $1/1260$ for $k = 2, 4$ and 6, respectively.

Table 1. ZFS parameters of Fe^{3+} ions in α-Al_2O_3.

g	b_2^0 (10^{-4} cm^{-1})	b_4^0 (10^{-4} cm^{-1})	b_4^3 (10^{-4} cm^{-1})	References
2.00	1683	−110	2181	[10]
2.00	1705	−108	2181	Our parameters

The spin Hamiltonian $\hat{\boldsymbol{H}}$ for ideal α-Al_2O_3:Fe^{3+} was of the following form:

$$\hat{\boldsymbol{H}} = \beta \vec{S} \cdot g \cdot \vec{B}_0 + \tfrac{1}{3} b_2^0 O_2^0 + \tfrac{1}{60}(b_4^0 O_4^0 + b_4^3 O_4^3)$$

with the first term representing the electronic Zeeman effect and the following terms concerning the ZFS part according to the space group symmetry $R\bar{3}c$ of the undisturbed matrix. The z axis lies along the unique threefold axis and the x axis has to be chosen such that b_4^{-3} vanishes. The exact computation of the spectrum has to be done over the x, y, z and $-x, y, z$ faces of the octahedron.

Based on a numerical diagonalization of the spin Hamiltonian, this code computes energy levels at any orientation, angular dependencies and the powder spectrum. It uses the partitioning and interpolating scheme developed by Alderman [23] which was originally devoted to compute NMR powder spectra and recently applied by Morin [10] for modelling EPR powder spectra. Broadening effects due to site to site distribution of the ZFS parameters are treated using first-order perturbation theory. In the code it is possible to take into account small distributions of any ZFS parameter. The distribution of each parameter b_k^q is characterized by a small perturbation quantity δb_k^q. Each perturbation quantity is considered as an individual perturbation Hamiltonian H_{pert}. For a given (m–n) transition involving m and n levels, the line broadening $\gamma_{mn}(\theta, \varphi)$ connected to H_{pert} is expressed as

$$\gamma_{mn}(\theta, \varphi) = 2 \left| \frac{\Delta E_m - \Delta E_n}{(\partial E_m / \partial H) - (\partial E_n / \partial H)} \right|$$

with $\Delta E_i = \langle V_i | H_{pert} | V_i \rangle$, where V_i is the eigenvector of the main Hamiltonian and $\partial E_i / \partial H$ is the local slope of the i level. In this way, the $\gamma_{mn}(\theta, \varphi)$ is the contribution of strain to the broadening, considered as symmetrical when the parameter deviates by $\pm \delta b_k^q$. Then δb_k^q may be seen as half the width of the corresponding b_k^q parameter distribution. All the other broadening effects, such as the natural linewidth, and the dipolar and hyperfine broadenings, are modelled by a constant linewidth Γ_0. Finally the full width at half maximum (FWHM) in the field domain is written: $\Gamma_{mn}(\theta, \varphi) = \sqrt{\Gamma_0^2 + \gamma_{mn}^2(\theta, \varphi)}$.

Roadmaps were calculated with the program EPR-NMR (version 6.4) [24].

By application of the superposition model [14–18], fluctuations in ZFS parameters were directly related to local geometrical changes in the neighbourhood of the transition metal ions.

3. Calculated EPR spectra: α-Al_2O_3:Fe^{3+}

Many different parameter sets describing the EPR spectrum of Fe^{3+} in alumina can be found in the literature [10, 25, 26]. The simulations presented in the following were obtained using the parameter set published recently by Morin and Bonnin [10] given in table 1.

3.1. Fe^{3+} ion on trigonal symmetry site

For Fe^{3+} ion in pure trigonal site symmetry, calculated S, X, K, Q and W spectra obtained with normal detection ($B_1 \perp B_0$) using the above-mentioned spin Hamiltonian parameters are

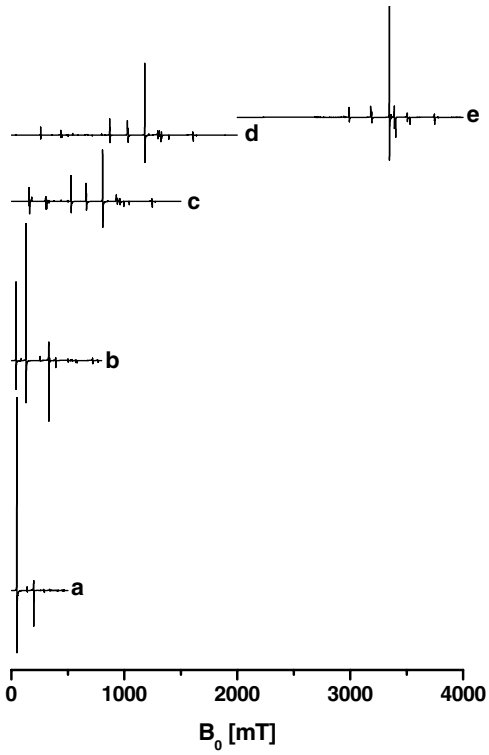

Figure 1. Calculated EPR spectra of α-Al_2O_3:Fe^{3+} powder showing the main transitions according to the microwave frequencies: (a) S-band (3.95 GHz); (b) X-band (9.33 GHz); (c) K-band (23.9 GHz); (d) Q-band (34.0 GHz); (e) W-band (94.0 GHz). The calculations were performed using the Morin parameter set [10] given in table 1 with a uniform linewidth Γ_0 of 1 mT.

gathered in figure 1. These calculations point out that, depending on the relation between the chosen microwave frequency and the actual ZFS parameters, different transitions dominate the spectra by their large intensities. In the following, the transitions are identified by the two levels (n–m) they connect, the levels being sorted from the largest to the smallest energy value. The S-band spectrum mainly determined by the (5–6) transition is typical of $H_{fs} \gg H_{Zeeman}$. The X-band is mainly composed of the (4–5), (5–6) and (3–4) transitions. At K- and Q-band frequencies even 'forbidden' transitions may gain a detectable intensity beside the (3–4) transition. At last, the spectrum expected at W-band is characteristic of a spin $S = 5/2$ fine structure acting as a perturbation of the Zeeman Hamiltonian.

3.2. Distributions of the ZFS parameters

As shown previously [5, 9–12], broadening effects of the EPR resonances observable in the experimental spectra cannot be accounted for by only varying the linewidth Γ_0, and finally discrepancies between the experimental spectra and those presented in figure 1 remain. Consequently, small fluctuations around the axial symmetry mirrored in the calculation by narrow distributions of the ZFS parameters around the 'perfect crystal' values may be invoked to explain these broadening effects. This is exemplified in figures 2–4. In figure 2 are presented roadmap calculations of single crystal line positions versus the rotation angle $\theta(B_0, z)$, in the xz plane with a variation of b_2^0 by $\pm 5\%$ corresponding to $b_2^0 = 1600$ and 1767×10^{-4} cm^{-1}

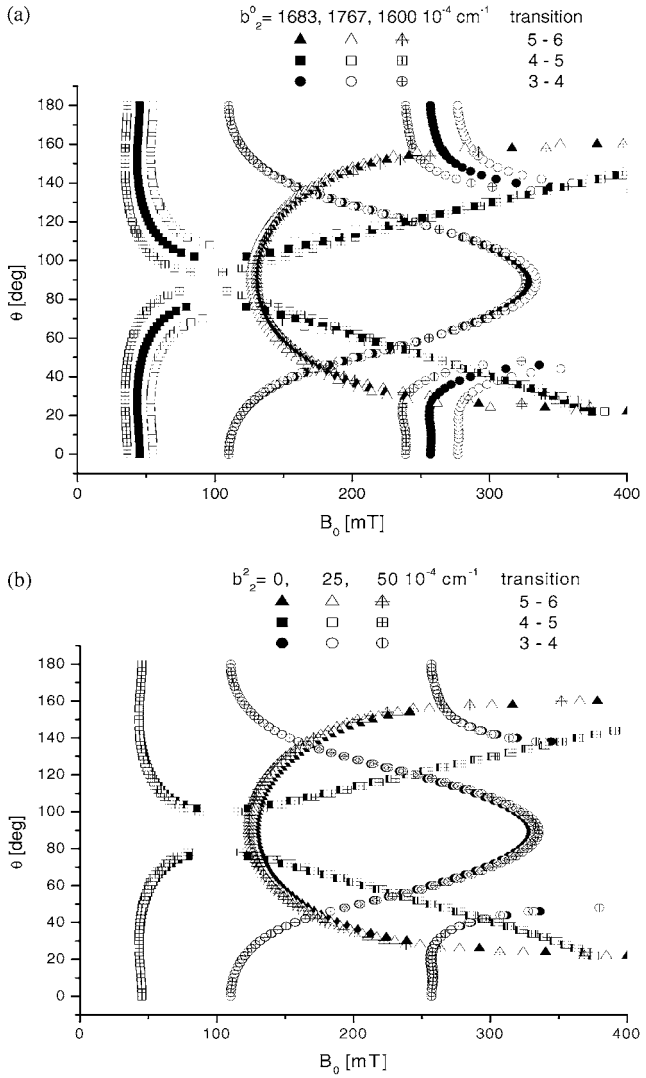

Figure 2. Roadmap calculations in X-band of single crystal line positions versus the rotational angle θ with: (a) variations of b_2^0 and (b) variations of b_2^2. The bold symbols are the values calculated using the Morin parameter set [10] given in table 1.

(figure 2(a)) and $b_2^2 = 0$, 25 and 50 $\times$ 10^{-4} cm^{-1} (figure 2(b)). It demonstrates that the individual transitions neither react in the same manner nor with the same sign on changes in the ZFS parameter. A variation of b_2^0 around the 'perfect crystal' value results in shifts of the main (5–6), (4–5) and (3–4) transitions whereas a variation of b_2^2 leads to splitting of the (5–6) and (3–4) transitions and leaves the (4–5) line position nearly unchanged. Then, a rather small b_2^2 distribution may result in a drastic change of relative line intensities and in an asymmetric broadening of the (5–6) transition (figure 3(b)), and a b_2^0 distribution may induce a more or less symmetric broadening of the transitions as shown on figure 3(c).

Although they are less striking, fingerprints of b_2^0 and b_2^2 distributions in Q-band are also evident in figure 4. As in X-band, a rather small b_2^2 distribution results in a change of the relative line intensities.

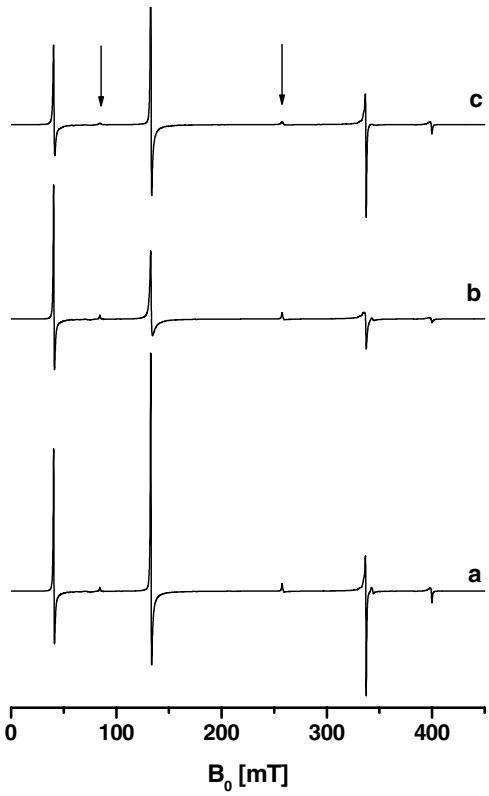

Figure 3. Influence of ZFS parameter distributions on the Fe^{3+} spectrum in corundum in X-band. The calculations are performed using the Morin parameter set [10] with a uniform linewidth Γ_0 of 1 mT. (a) Calculated without ZFS distribution; (b) b_2^2 distribution: $\delta b_2^2 = 20 \times 10^{-4}$ cm^{-1}; b_2^0 distribution: $\delta b_2^0 = 5 \times 10^{-4}$ cm^{-1}. Arrows indicate lines which are broadened by very narrow b_2^0 distributions.

Other computations allow us to conclude that the experimental peak to peak linewidth of the low field line in X-band is nearly equal to the Γ_0 parameter introduced in the calculation, whatever the b_2^2 distribution is and if $\delta b_2^0 = 0$. Computations show also that changes in relative intensities occur as soon as δb_2^2 is of the order of Γ_0. On the other hand, the small sharp lines indicated by an arrow in figures 3 and 4 are shown to be severely broadened by a very small b_2^0 distribution. At last, it may be outlined that the Fe^{3+} EPR spectrum in corundum is much less sensitive to variations of the fourth-order ZFS parameters b_4^q. This is the reason why, in the following, we will concentrate on the second-order ZFS parameters.

From these foregoing investigations, it appears that changes in the EPR spectra may allow us to extract valuable information on the probe neighbourhood through the variation of the second-order ZFS parameters.

4. Experimental EPR spectra and spin Hamiltonian parameters: dependence on the sample preparation route

In the following, we adjust experimental and calculated spectra in order to determine the linewidths and lineshapes, the ZFS parameter set and their distributions for samples obtained through different preparation routes.

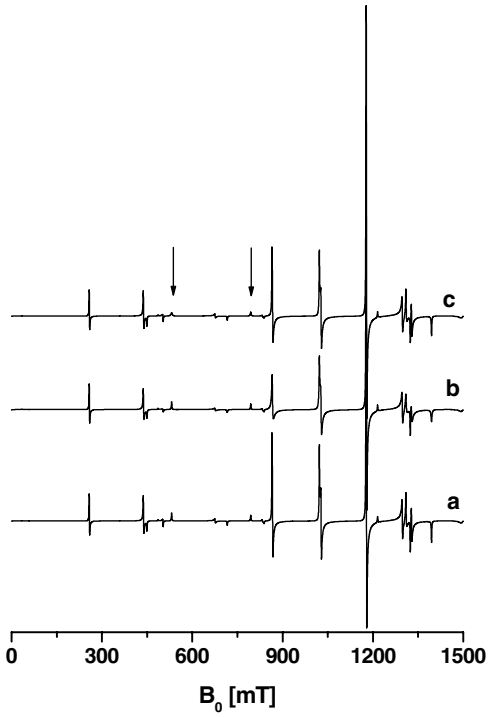

Figure 4. Influence of ZFS parameter distributions on the Fe^{3+} spectrum in corundum in Q-band. The calculations are performed using the Morin parameter set [10] with a uniform linewidth Γ_0 of 2 mT. (a) Calculated without ZFS distribution; (b) b_2^2 distribution: $\delta b_2^2 = 20 \times 10^{-4}$ cm^{-1}; (c) b_2^0 distribution: $\delta b_2^0 = 5 \times 10^{-4}$ cm^{-1}. Arrows indicate lines which are broadened by very narrow b_2^0 distributions.

4.1. α-Al_2O_3:Fe^{3+}, sample I

In order to discuss the EPR experimental response of Fe^{3+} ions in corundum powders prepared via different routes, one has to consider first of all the formally undisturbed powder. It should fulfil the following requirements:

(i) the main fraction of the crystallites has to be large enough to reduce surface effects to a negligible minimum,
(ii) the individual crystallites should have a minimum of lattice defects—their quality might be improved by thermal annealing,
(iii) the concentration of Fe^{3+} should be chosen as low as possible in order to reduce both the formation of pairs and magnetic clusters. Thus, the distortion of the matrix by chemically induced stress and the influence of dipole–dipole interactions on the relaxation behaviour and the linewidths of EPR signals should be neglected.

Sample I contains about 2 ppm Fe^{3+}, which is sufficient to allow EPR detection in all frequency bands from S- to W-band. X-ray diffraction yields an average particle diameter of 350 nm.

The experimental EPR spectra of this sample as obtained in X-, Q- and W-bands are shown in figure 5. Simulations were performed to obtain a set of parameters as a starting point for the investigation of the sol–gel powders as well as of the mechanically and thermally treated

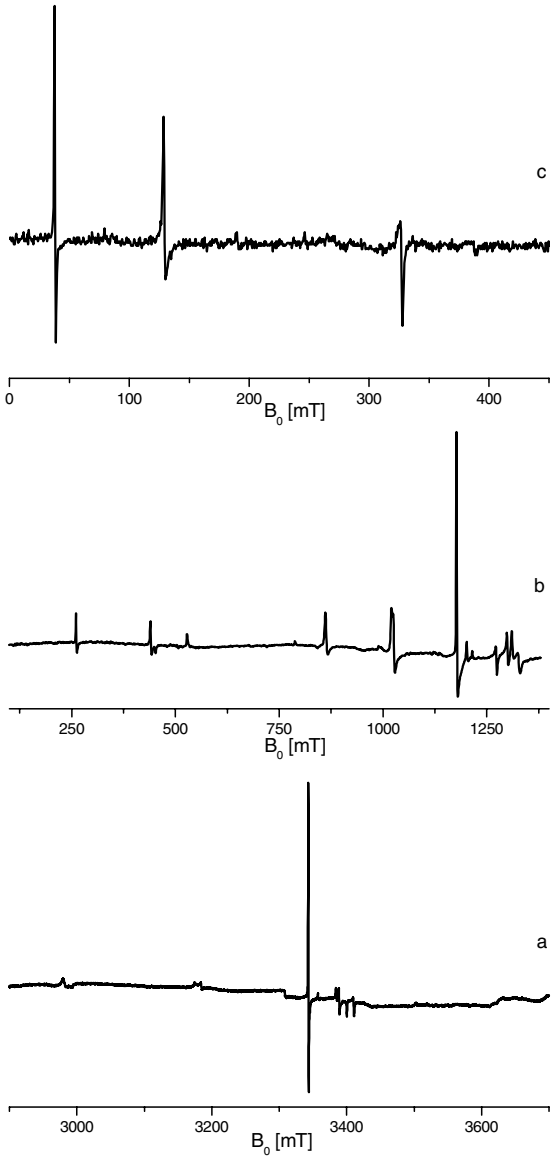

Figure 5. Experimental spectra of an α-Al_2O_3:Fe^{3+} powder (sample I): (a) W-band (94.0 GHz, 10 K); (b) Q-band (34.0 GHz, 77 K); (c) X-band (9.33 GHz, 293 K).

ones. The simulations giving the best reproduction of the line positions in all frequency bands (and with different simulation programs [11, 21, 24]) were obtained by slightly adjusting the parameter set published by Morin and Bonnin [10] (table 1) and are presented in figures 6(a) and 7(a) for X- and Q-bands, respectively. A Gaussian lineshape was applied in agreement with low Fe^{3+} concentration [27, 28]. A linewidth $\Gamma_0 = 1.5 \pm 0.5$ mT was used for all the microwave frequencies. Comparing this linewidth with the data published by Bogle and Symmons [2] for a single crystal study (0.6 mT for a sapphire containing 0.005 ionic % of Fe^{3+}) and keeping in mind the increasing linewidth with decreasing particle size and increasing

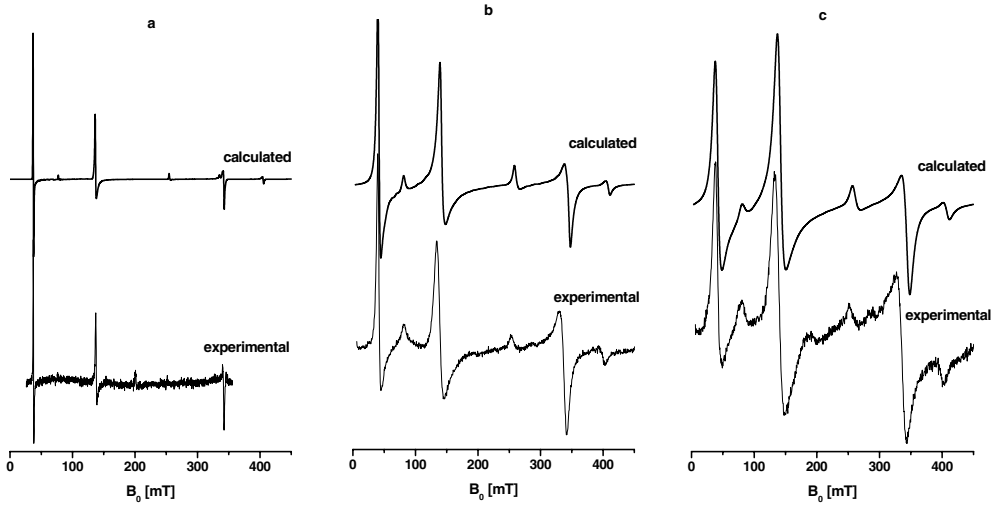

Figure 6. Experimental and calculated X-band EPR spectra of Fe^{3+} in different samples of α-Al_2O_3. The calculations are performed using our ZFS parameter set given in table 1. The linewidths Γ_0 and the b_2^2 distributions are given in table 2 for the different samples: (a) sample I; (b) sample III; (c) sample V.

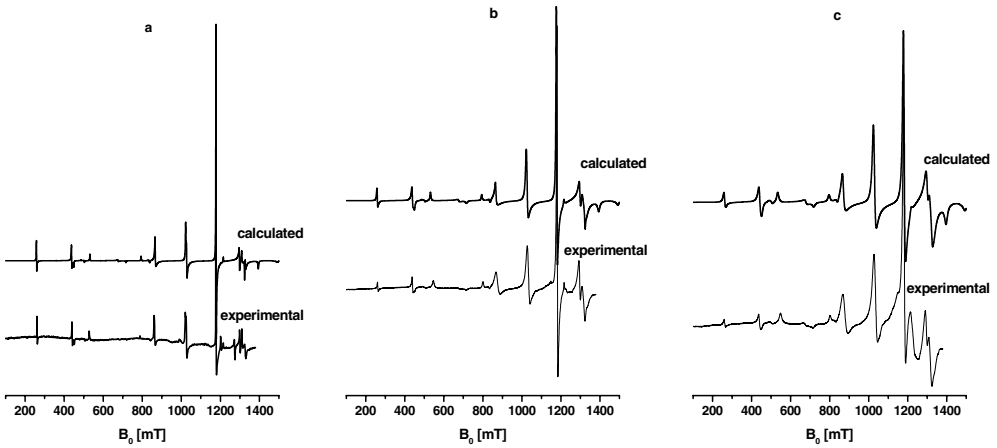

Figure 7. Experimental and calculated Q-band EPR spectra of Fe^{3+} in different samples of α-Al_2O_3 using the same parameters as given in the caption of figure 6: (a) sample I; (b) sample III; (c) sample V.

concentration (de Biasi and Rodrigues [7, 8]) we conclude that our sample I fulfils at least the requirements (i) and (iii) (*vide infra*).

The ZFS parameter distributions were determined as: $\delta b_2^0 = 0$ (the small lines are not broadened, see 3–2) and $\delta b_2^2 = 25 \times 10^{-4}\,\mathrm{cm}^{-1}$. The corresponding EPR spectra are presented in figures 6(a) and 7(a).

Our results concerning the commercial corundum powder (sample I) are in agreement with those obtained by Morin *et al* [10] and Boizot [9]. They give evidence for a slightly rhombic distortion of the oxygen octahedra.

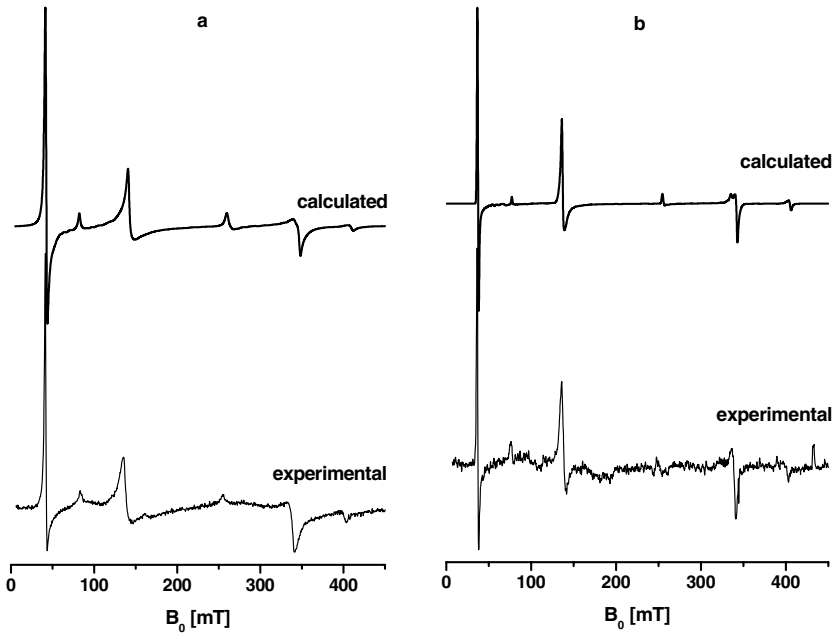

Figure 8. Experimental and calculated X-band EPR spectra of Fe^{3+} in unannealed (a) and annealed (b) sample II of α-Al_2O_3. The calculations are performed using our ZFS parameter set given in table 1. The linewidths Γ_0 and the b_2^2 distributions are given in tables 2 and 4.

Table 2. Doping levels, EPR lineshapes and linewidths and widths of the b_2^2 distributions of the corundum samples I–V.

Sample	Fe_2O_3 (mol%)	EPR lineshape	EPR linewidth Γ_0 (mT)	δb_2^2 (10^{-4} cm^{-1})
I	0.0002	Gaussian	1.5 ± 0.5	25 ± 5
II	0.02	Gau/Lor[a]	3.0 ± 0.5	140 ± 10
III	0.26	Lorentzian	6.0 ± 1.0	80 ± 10
IV	0.52	Lorentzian	8.0 ± 1.0	80 ± 10
V	1.04	Lorentzian	13.0 ± 1.0	80 ± 10

[a] The best agreement between the calculated and experimental spectra is obtained for a linear combination of normalized Gaussian (0.5) and Lorentzian (0.5) functions with the same width Γ_0.

Transitions belonging to Fe^{3+} pairs as described by Bramley and McCool [29] have not been detected in sample I. They seem to be very unlikely, since by assuming a statistical distribution of iron in the lattice and following the estimation of Gunsser *et al* [30] the ratio between the signals of Fe^{3+} pairs and isolated Fe^{3+}, respectively, is expected to be of the order of 10^{-6}.

4.2. Sample II

For this sample, a comparison between experimental and calculated spectra is presented in figures 8(a) for X-band. The spin Hamiltonian parameter set used is the same as for sample I (see table 2). The broadening of the experimental lines prevents us from a more precise determination. However, the linewidth Γ_0 and the distributions of ZFS can be accurately

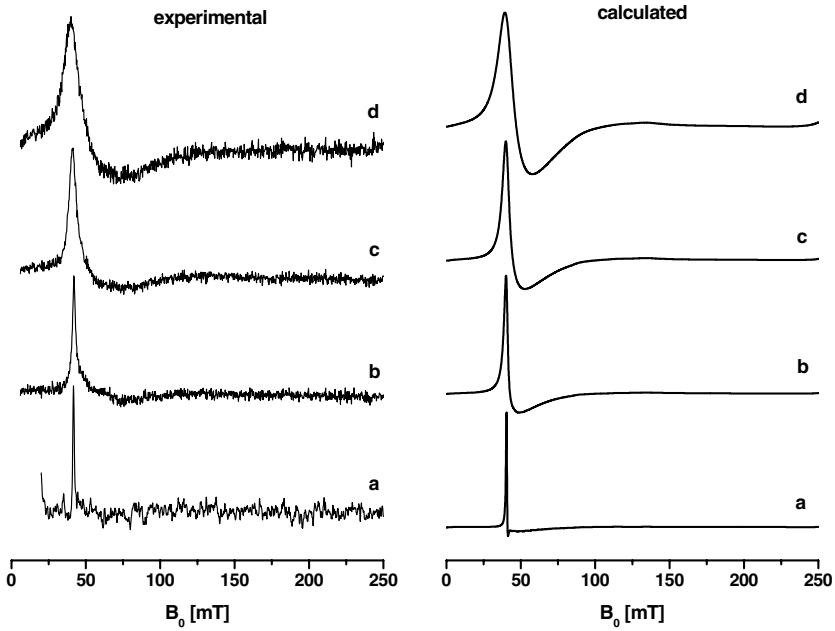

Figure 9. Experimental and calculated spectra for parallel detection in X-band ($B_1 \parallel B_0$) for (a) sample I; (b) sample II; (c) sample III; (d) sample V.

determined from the spectra. The results are given in table 2. The lineshape no longer seems Gaussian but the Lorentzian shape is not completely satisfying, especially for X-band spectra. The linewidth is larger than in sample I. As for sample I, no distribution of the axial b_2^0 has to be invoked ($\delta b_2^0 = 0$) but the distribution of b_2^2 is quite important ($\delta b_2^2 = 140 \times 10^{-4}\ \mathrm{cm}^{-1}$). This gives evidence for a rhombic distortion of the oxygen octahedra stronger than in sample I.

4.3. Samples III, IV and V

For samples III and V, comparison between experimental and calculated spectra are presented in figures 6(b), (c) for X-band and 7(b), (c) in Q-band. As for sample II, the parameter set used is the same as for sample I. Linewidths Γ_0, lineshapes and distributions of ZFS determined from the spectra are gathered in table 2 for the three samples. Linewidths appear to be strongly dependent on the Fe^{3+} doping level. No distribution of the axial b_2^0 has to be invoked ($\delta b_2^0 = 0$) and the same δb_2^2 is found whatever the Fe^{3+} concentration ($0.26 \leqslant c_{Fe^{3+}} \leqslant 1.04$ (mol% Fe_2O_3)). This gives evidence that the observed rhombic distortion of the oxygen octahedra measured by δb_2^2 is related to the preparation route.

4.4. Mechanically milled 99.99% α-Al_2O_3

X-band measurements at room temperature have been reported elsewhere (see figure 9 in [5]). Γ_0 and δb_2^2 values, obtained through simulation of the experimental spectra measured at short milling time, are given in table 3. The δb_2^2 values increase rapidly with the milling time whereas the linewidths Γ_0 are only slightly affected. This indicates that the mechanical milling modifies the local structure around the paramagnetic probe and that the grain size does not have a large contribution to the intrinsic linewidth Γ_0.

Table 3. Mean grain sizes, EPR linewidths and widths of the b_2^2 distribution of milled α-Al_2O_3 (sample I).

Milling time (min)	Mean grain size (nm)[a]	EPR linewidth Γ_0 (mT)	δb_2^2 (10^{-4} cm^{-1})
0	350	1.0 ± 0.3	25 ± 5
10	130	1.5 ± 0.3	40 ± 10
20	90	1.5 ± 0.3	60 ± 10

[a] Grain size as determined by x-ray [5].

Table 4. EPR linewidths and widths of the b_2^2 distribution of thermally annealed α-Al_2O_3.

Sample	EPR linewidth Γ_0 (mT)	δb_2^2 (10^{-4} cm^{-1})
I	1.2 ± 0.5	30 ± 5
II	1.6 ± 0.5	35 ± 5

4.5. Thermally treated samples (samples I and II)

The results obtained for these two samples after thermal treatment are given in table 4. The lineshape appears to be Gaussian. The parameters remain nearly the same for sample I whereas they have to be strongly modified for sample II. A comparison between unannealed and annealed sample II is done in figure 8. Whereas for sample I the calculation of the EPR spectra is possible with nearly the same linewidth Γ_0 and δb_2^2 distribution as in the unannealed case (see table 2), a marked decrease of the width of the b_2^2 distribution from 140 to 35×10^{-4} cm^{-1} is observed for sample II (see figures 8(a), (b)). This result underlines again our findings (cf 4.1) that sample I is already a powder of good crystallinity and no spectacular changes can be expected after thermal annealing. However, in the case of sample II the matrix is much more improved after thermal annealing including a smaller number of lattice defects. From the viewpoint of Fe^{3+} ions it may be concluded that the extension of the δb_2^2 distribution mirrors the quality of the crystalline phase: the smaller δb_2^2, the better the quality.

At this point it should be mentioned that a partial recrystallization around Fe^{3+} ions could be observed after thermal annealing even in sample I milled for 60 h (see [5]).

4.6. Parallel mode detection (samples I, II, III and V)

The X-band spectra obtained with parallel mode detection ($B_1 \parallel B_0$) for the different samples are shown in figure 9. The spectrum of sample I was first published by Scholz and Stösser [31]. The experimental spectra are well reproduced, applying the parameter sets deduced from the normal mode detection spectra (cf figure 9 and tables 1 and 2). From these reconstructions it may be concluded that the peak to peak experimental width of the EPR line does not depend on the δb_2^2 distribution width.

Since the spectra obtained by the two different detection modes in X-band have to be described by the same Hamiltonian, the detection in the parallel mode ($B_1 \parallel B_0$) will give specific additional information about the interacting spin system. It concerns the degree of mixing of eigenstates and a verification of the interpretation of the data obtained by the usual perpendicular detection for the samples used in this contribution.

5. Relation between spin Hamiltonian parameters, linewidths and local order

5.1. Relation between EPR linewidths, lineshapes and Fe^{3+} concentration

From the results described above, it is found that, for Fe^{3+} low doping level $\leqslant 0.02$, the lineshape is rather Gaussian and the linewidth Γ_0 is small and about 1.5 mT in any case. It corresponds nearly to the residual linewidth due to interaction between the Fe spins and the neighbouring aluminium nuclei.

For samples III, IV and V for which the Fe concentration is much higher (0.26–1.04 mol% Fe_2O_3), a Lorentzian lineshape gives the best adjustment between experimental and calculated spectra. This is in agreement with broadening due to Fe–Fe interactions [27, 28]. Furthermore, a linear dependence of the linewidth on the concentration can be determined which is expressed according to the following formula:

$$\Gamma_0 \text{ (mT)} = 3.5 + 9.1\text{c (mol\%)}.$$

For vanishing Fe^{3+} concentration c a residual linewidth Γ_0 of 3.5 mT is determined, which is a bit larger than that deduced from the measurements on samples I and II. This might be in part caused by the change of the lineshape.

The EPR measurements on the milled samples lead to the conclusion that the linewidths Γ_0 appear to be not really sensitive to the grain size, at least at low milling time. This may be understood if we assume that the EPR signal originates mainly from Fe^{3+} ions situated inside the grains exclusively and not at the surface of the grains.

5.2. Relation between ZFS parameter distributions and local order around Fe^{3+}

From our simulations it appears that in all the samples and even in sample I (99.99% α-Al_2O_3, un- or less-disturbed powder), the spectrum of Fe^{3+} is best simulated by admitting a small distribution of b_2^2 (see also [5]). This is characteristic of a rhombic distortion. Another result has to be noticed: the b_2^0 parameter must not be distributed. Following that, the implementation of paramagnetic Fe^{3+} ions into the diamagnetic corundum matrix leads obviously to a local decrease of the site symmetry of the host site from the $R\overline{3}c$ axial symmetry [5]. Our results demonstrate that this distortion is dependent on the preparation route and on the thermal and mechanical treatment.

The local distortion can be quantitatively estimated with the help of the superposition model [14–18] directly relating ZFS parameters to bond lengths and angles. This model assumes that the spin Hamiltonian parameters b_k^q result from linear superposition of single ligand contributions of the form: $b_k^q = \sum_i \overline{b}_k(R_i) K_k^q(\Theta_i, \Phi_i)$. The $K_k^q(\Theta_i, \Phi_i)$ are spherical harmonic functions of rank k of the polar angles. The $\overline{b}_k(R_i)$ are functions of the radial metal–ligand distances R_i. They are called intrinsic parameters and differ for various paramagnetic ions as well as for various ligands.

In the following, we restrict the discussion to the second-order fine structure parameters. The summation goes over the nearest neighbours of the paramagnetic ion. In the most general case we have five b_2^q parameters:

$$b_2^0 = \tfrac{1}{2} \sum_i \bar{b}_2(R_i)(3\cos^2\Theta_i - 1)$$

$$b_2^{\pm 1} = 3 \sum_i \bar{b}_2(R_i) \sin 2\Theta_i \left\{ \begin{matrix} \cos \Phi_i \\ \sin \Phi_i \end{matrix} \right\}$$

$$b_2^{\pm 2} = \tfrac{3}{2} \sum_i \bar{b}_2(R_i) \sin^2 \Theta_i \left\{ \begin{matrix} \cos 2\Phi_i \\ \sin 2\Phi_i \end{matrix} \right\}$$

where Θ_i are the angles between the z axis and the different metal–ligand bonds and Φ_i are those between the projections of these metal–ligand bonds into the $\{x, y\}$ plane and the x axis. Note that the b_2^{-q} are obtained by changing $\cos(a\Phi)$ by $\sin(a\Phi)$.

In the case of Fe^{3+} in $R\overline{3}c$ trigonal symmetry, the polar coordinates of the six nearest ligands can be expressed with only two metal–ligand distances r_1 and r_2, two angles between the R_i direction and the z threefold axis θ_1 and θ_2 and six Φ_i angles between the projections of the Fe–O bonds which depend also on two angular values φ_1 and φ_2:

$$R_{1,2,3} = r_1, \qquad R_{4,5,6} = r_2, \qquad \Theta_{1,2,3} = \theta_1, \qquad \Theta_{4,5,6} = \theta_2$$
$$\Phi_1 = \varphi_1, \qquad \Phi_2 = \varphi_1 + \frac{2\pi}{3}, \qquad \Phi_3 = \varphi_1 + \frac{4\pi}{3}, \qquad \Phi_4 = \varphi_2,$$
$$\Phi_5 = \varphi_2 + \frac{2\pi}{3} \qquad \text{and} \qquad \Phi_6 = \varphi_2 + \frac{4\pi}{3}.$$

Then, the second-order ZFS parameters are given by

$$b_2^0 = \tfrac{3}{2}\bar{b}_2(r_1)(3\cos^2\theta_1 - 1) + \tfrac{3}{2}\bar{b}_2(r_2)(3\cos^2\theta_2 - 1)$$
$$b_2^1 = 9\bar{b}_2(r_1)\sin 2\theta_1 \sum_{i=1}^{3}\cos\Phi_i + 9\bar{b}_2(r_2)\sin 2\theta_2 \sum_{i=4}^{6}\cos\Phi_i$$
$$b_2^2 = \tfrac{9}{2}\bar{b}_2(r_1)\sin^2\theta_1 \sum_{i=1}^{3}\cos 2\Phi_i + \tfrac{9}{2}\bar{b}_2(r_2)\sin^2\theta_2 \sum_{i=4}^{6}\cos 2\Phi_i.$$

Using a R_{Fe-O} distance of 1.98 Å, the distances r_i and θ_i angles of the corundum matrix extracted from our recent high resolution x-ray measurements [5][4], and a two-exponential form for the calculation of $\bar{b}_2(R_i)$ [9]:

$$\bar{b}_2(R_i) = -A\left(\frac{R_0}{R_i}\right)^m + B\left(\frac{R_0}{R_i}\right)^n$$
$$\text{with } A = 0.68\ \text{cm}^{-1},\ B = 0.27\ \text{cm}^{-1},\ m = 10,\ n = 13,$$

calculations allowed the determination of $b_2^0 = 0.1708\ \text{cm}^{-1}$. This is very close to the experimental value of $b_2^0 = 0.1705\ \text{cm}^{-1}$. From this agreement, we can conclude that the Fe^{3+} ions substitute the Al^{3+} ones. From our point of view, it is not necessary to invoke displacement of the Fe^{3+} as in [18] to account for the b_2^0 value. Moreover, whatever the values of φ_1 and φ_2 (in α-Al_2O_3, we found $|\varphi_1 - \varphi_2| = 3.76°$), $b_2^{\pm1}$ and $b_2^{\pm2}$ equal to zero.

The interpretation of the width of the distribution of rhombic distortions measured by $2\delta b_2^2$ is not straightforward because several different possibilities may correspond to a decrease of the local symmetry. However, the simulations of the experimental spectra show unambiguously the absence of a b_2^0 distribution. From this result, we may assume that there is neither variation of the R distances nor of the Θ angles. Then, if this assumption is correct, the only way to explain the rhombic distortion of the AlO_6 octahedra is to relate it to changes in the Φ angles. From the above formulae, it is easily seen that $b_2^{\pm1}$ and $b_2^{\pm2}$ are different from zero only if the threefold periodicity of the Φ values is broken. That is to say, if the oxygen triangles are no longer equilateral. Even in that case the quantification of the distortion is not unique. Nevertheless, an upper limit of the distortion can be inferred, assuming that only one oxygen atom moves as in [5]. The decrease of the local site symmetry will be explained by the distribution of one Φ angle whose width is given by $2\delta\Phi$. The relation between a $\delta\Phi$ value and the corresponding b_2^2 parameter is obtained in the following way: firstly, the five components

[4] Al–O distances and angles θ in α-Al_2O_3: $r_1 = 1.975$ Å, $r^2 = 1.853$ Å, $\theta_1 = 47.74°$, $\theta_2 = 63.12°$. (θ:∠ (c axis, Fe–O)).

Table 5. Application of the superposition model for the determination of the $\delta\varphi$ distribution.

δb_2^2 (10^{-4} cm^{-1})	25	30	40	60	80	140
$\delta\Phi_{1,2 \text{ or } 3}$ (deg)	0.21	0.25	0.33	0.5	0.67	1.17
$\delta\Phi_{4,5 \text{ or } 6}$ (deg)	0.09	0.11	0.14	0.21	0.28	0.49

of the second-order fine structure tensor b_2^0, $b_2^{\pm 1}$ and $b_2^{\pm 2}$ are calculated according to the above-mentioned formulae in the reference axes related to the original local structure; secondly, the three eigenvalues are calculated and finally the b_2^0 and b_2^2 parameters in the new eigenaxes are extracted from the eigenvalues. These are the parameters which have to be compared to the corresponding measured ones. The calculated $\delta\Phi$ values are found to be related to the half-width δb_2^2 of the b_2^2 parameter distribution according to the following formulae:

$$\delta b_2^2 \ (10^{-4} \text{ cm}^{-1}) = 120.0|\delta\Phi_{1,2 \text{ or } 3}| \text{ (deg)}$$

and

$$\delta b_2^2 \ (10^{-4} \text{ cm}^{-1}) = 283.3|\delta\Phi_{4,5 \text{ or } 6}| \text{ (deg)}.$$

Table 5 gives the $\delta\Phi$ corresponding to the experimental δb_2^2 values. It is worthwhile noting that the strong alterations of the spectra are related to quite small angular fluctuations ($<1.5°$) and that the smaller the Fe–O distance, the larger the effect.

6. Conclusions

EPR experiments on a multi-frequency scale combined with parallel mode detection at X-band as well as extensive simulations were performed on α-Al_2O_3 powders using Fe^{3+} as a local probe. The linewidths, lineshapes, the spin Hamiltonian parameters and their distributions were determined for different powder samples prepared by different routes and/or modified by thermal or mechanical treatments, with different doping levels and grain sizes. The applied procedure presents the advantage of discriminating broadening effects due to slight variations of the electronic environment from site to site (random field gradients [32]) from the other contributions to the linewidth.

The different sensitivity of the individual transitions on ZFS parameter distributions allows us to separate changes in b_2^0, and b_2^2 when leaving the 'undisturbed' system and investigating the influence of thermally or mechanically induced changes. Since this sensitivity is dependent on the measuring frequency, for each ZFS parameter set there exists an optimal EPR frequency—not necessarily the highest available—for separation of individual distributions. For Fe^{3+} ions in corundum, the widely used X-band frequency is well adapted.

The main conclusions are the following:

(i) The simulation of the EPR spectra of low-level doped corundum powders (sample I) has to be performed with a Gaussian lineshape with a 1.5 mT residual Γ_0 linewidth due to interaction between Fe spins and Al nuclei.

(ii) At higher concentrations ($>0.02\%$), a Lorentzian lineshape is required. The dipolar broadening of the linewidths Γ_0 of different samples is directly proportional to the concentration of the Fe^{3+} ions, whereas the influence of the grain size (maximum values at $\sim$350 nm, see milled samples) is negligible.

(iii) A detailed analysis of the relative intensities of the allowed and 'forbidden' spin transitions of Fe^{3+} ions in 'as-obtained' corundum powders as well as in thermally and mechanically treated ones yielded the need to extend the determined ZFS parameter set by a distribution

of b_2^2. It corresponds to a distribution of rhombic distortions reducing the local Fe^{3+} site symmetry. For each studied sample, the width of this distribution was quantitatively measured by δb_2^2. The observed dependence of this parameter on the preparation routes and on the thermal and mechanical treatments proves that it may be seen as an overall qualitative estimation of the proportion of structural lattice defects or of the crystalline quality of the sample. The best crystalline quality is observed for sample I from Aldrich with the smallest δb_2^2 value, the worse one to sample II from Alcoa before thermal annealing, the sol–gel materials being of intermediate quality.

(iv) These lattice distortions may be tentatively related to several origins: first, the Fe^{3+} ions adapt their local surroundings when substituting for Al^{3+}; second, local strains are not fully relaxed due to insufficiently long thermal annealing of the synthesized corundum powders or are induced by mechanical milling treatment.

(v) Using the superposition model we tried to get a quantitative description of the degree of local distortion in all samples. The simplest assumption in agreement with the experimental results leads to the conclusion that, whatever the sample, the resulting local distortion involves neither Fe–O distance nor polar angle modifications but only breaking of the threefold symmetry of the oxygen arrangement around the paramagnetic probe. Then, the distribution of ZFS parameters is interpreted in terms of Φ angle distributions. The results indicate that cw-EPR spectroscopy is sensitive to variations of bond angles of less than 0.1°.

(vi) An important application of this work would be to use the described procedure for modified alumina but also for crystalline powders where slight disorder is always more or less present to gain more precise information about the crystalline quality in relation to the preparation route.

Acknowledgments

This work is partially supported by the PROCOPE program. Dr A Zehl is gratefully acknowledged for experimental assistance. We thank Dr W Hofbauer and Dr F Lendzian (Technical University of Berlin) for performing W-band measurements.

References

[1] Klein H, Scherz U, Schulz M, Setyono H and Wisznewski K 1977 *Z. Phys.* B **28** 149
[2] Bogle G S and Symmons H F 1958 *Proc. Phys. Soc.* A **73** 531
[3] Symmons H F and Bogle G S 1962 *Proc. Phys. Soc.* **79** 468
[4] Schulz-Du Bois E O 1959 *Bell Syst. Tech. J.* **38** 271
[5] Scholz G, Stösser R, Klein J, Silly G, Buzaré J Y, Laligant Y and Ziemer B 2002 *J. Phys.: Condens. Matter* **14** 2101
[6] de Biasi R S and Rodrigues D C S 1981 *J. Mater. Sci.* **16** 968
[7] de Biasi R S and Rodrigues D C S 1983 *J. Mater. Sci. Lett.* **2** 210
[8] de Biasi R S and Rodrigues D C S 1985 *J. Am. Ceram. Soc.* **68** 409
[9] Boizot B 1996 *Thesis* Université Pierre et Marie Curie, Paris
[10] Morin G and Bonnin D 1999 *J. Magn. Reson.* **136** 176
[11] Scholz G, Stösser R, Krossner M and Klein J 2001 *Appl. Magn. Reson.* **21** 105
[12] Priem A, van Bentum P J M, Hagen W R and Reijerse E 2001 *Appl. Magn. Reson.* **21** 535
[13] Kaminskii A 1990 *Laser Crystals* (Berlin: Springer)
[14] Newman D J and Urban W 1972 *J. Phys. C: Solid State Phys.* **5** 3101
[15] Siegel E and Müller K A 1979 *Phys. Rev.* B **19** 109
[16] Müller K A, Berlinger W and Blazey K W 1987 *Solid State Commun.* **61** 21
[17] Hemig M and Lehmann G 1987 *Electronic Magnetic Resonance of the Solid State* ed J A Weil (Ottawa: Canadian Society for Chemistry) p 163

[18] Zheng W C 1998 *Physica* B **245** 119
[19] Yoldas B E 1975 *Am. Ceram. Soc. Bull.* **54** 286
[20] Yoldas B E 1975 *J. Mater. Sci.* **10** 1856
[21] Buzaré J Y, Legein C, Silly G and Emery J 2001 *OHD Proc. (Le Mans, 2001)* p 37
[22] Rudowicz C 1985 *J. Phys. C: Solid State Phys.* **18** 1415
[23] Aldermann D W, Solum S M and Grant D M 1986 *J. Magn. Reson.* **99** 3717
[24] Mombourquette M J, Weil J A and McGavin D G 1993 *Computer program EPR-NMR (ver. 6.4, 2000)* Department of Chemistry, University of Saskatchewan, Canada
[25] Stößer R, Steinfeldt N, Brenneis R and Nofz M 1996 *J. Mater. Sci.* **31** 1405
[26] Kuska H A and Rogers M T 1970 *Electron Spin Resonance of First Row Transition Metal Complex Ions* (Moscow: Mir) p 85
[27] Kittel C and Abrahams E 1953 *Phys. Rev.* **90** 238
[28] Grant W J C and Strandberg M W P 1964 *Phys. Rev.* **135** A727
[29] Bramley R and McCool M B 1976 *J. Phys. C: Solid State Phys.* **9** 1793
[30] Gunsser W, Oechssler D and Knappwost A 1967 *Z. Phys. Chem. (Wiesbaden)* **54** 31
[31] Stösser R and Scholz G 1998 *Appl. Magn. Reson.* **15** 449
[32] Stoneham A M 1969 *Rev. Mod. Phys.* **41** 82